Online-Journals.org

iJOE International Journal of Online and Biomedical Engineering

iJOE | eISSN: 2626-8493 | Vol. 21 No. 7 (2025) | OPEN ACCESS

https://doi.org/10.3991/ijoe.v21i07.54439

PAPER

Illumination-Robust Conjunctival Image Preprocessing for Accurate Segmentation and Anemia Detection Using Deep Learning

Jose Humberto Fuentes-Beingolea[1](✉), Facundo Palomino-Quispe[1], Julio Cesar Herrera-Levano[1], Willy Vargas-Mateos[1], Ruben Florez[1], Ana Beatriz Alvarez[2]

[1]LIECAR Lab, Universidad Nacional de San Antonio Abad del Cusco, Cusco, Perú

[2]PAVIC Lab, Universidade Federal do Acre, Acre, Brasil

131358@unsaac.edu.pe

ABSTRACT

Anemia, defined by reduced hemoglobin or red blood cell levels, remains a critical public health issue, particularly in resource-limited settings where traditional diagnostics are inaccessible. Non-invasive detection via ocular conjunctiva imaging offers a viable solution but is challenged by illumination variability in outdoor environments. This study introduces a novel preprocessing pipeline to standardize conjunctival images, employing grayscale histogram normalization, LAB color space-based glare inpainting, and adaptive contrast enhancement to counter uneven lighting and reflections. Segmentation performance was assessed using U-Net, BiSeNet, and ConjunctiveNet; U-Net outperformed the others, achieving a precision of 84.22% with preprocessing versus 80.08% without preprocessing. For anemia classification, an artificial neural network (ANN), CNN-ResNet, and SLIC-GAT models were tested on the CP-AnemiC (Ghana) and Eyes-defy-anemia (India) datasets. Preprocessing significantly boosted ANN accuracy from 81.54% to 85.51% (Ghana) and 85.94% to 88.28% (India), with precision increasing by up to 6.33%. For CNN-ResNet, F1-scores improved from 81.91% to 89.15% (Ghana), while for ANN on the India dataset, F1-scores increased from 85.73% to 87.35%. These results highlight the pipeline's ability to enhance segmentation accuracy and classification reliability, reducing false positives and enabling robust anemia detection under variable lighting, thus advancing non-invasive diagnostics for field applications.

KEYWORDS

anemia, deep learning, non-invasive diagnosis, luminance correction processing, illumination variability

1 INTRODUCTION

The World Health Organization (WHO) [1] defines anemia as a clinical condition marked by a reduction in red blood cell count or hemoglobin levels, the protein

Fuentes-Beingolea, J.H., Palomino-Quispe, F., Herrera-Levano, J.C., Vargas-Mateos, W., Florez, R., Alvarez, A.B. (2025). Illumination-Robust Conjunctival Image Preprocessing for Accurate Segmentation and Anemia Detection Using Deep Learning. *International Journal of Online and Biomedical Engineering (iJOE)*, 21(7), pp. 106–124. https://doi.org/10.3991/ijoe.v21i07.54439

Article submitted 2025-01-15. Revision uploaded 2025-03-28. Final acceptance 2025-03-28.

essential for oxygen transport from the lungs to the body's tissues. Insufficient hemoglobin hinders the blood's oxygen-carrying capacity, potentially causing symptoms like fatigue, weakness, dizziness, and shortness of breath. Anemia arises from various causes, including nutritional deficiencies, infections, inflammation, chronic illnesses, and inherited conditions. A substantial public health concern, anemia disproportionately impacts vulnerable groups such as young children, women of reproductive age, pregnant women, and new mothers [2]. Beyond direct effects on physical health, anemia impairs cognitive and physical development in children and reduces work productivity in adults, generating adverse economic and social outcomes. In children, anemia can impede cognitive and physical development, affecting their academic achievements long-term. Additionally, it is linked to severe complications such as low birth weight and elevated maternal and child morbidity and mortality rates [1].

Anemia can manifest with varying visual characteristics in the human body, the severity of which is directly related to its impact on red blood cells. A primary visible indicator of anemia is clinical pallor, including paleness of the skin, palm surfaces, nail beds, and ocular conjunctiva. The specific hue and intensity of this pallor fluctuate depending on the condition's severity and associated symptoms [3].

The diagnostic process for anemia involves a thorough evaluation by a healthcare professional. This includes gathering information on the patient's risk factors and conducting blood tests for confirmation [1]. A physical examination is also crucial to identify potential signs of anemia, such as pallor in specific body areas, weakness, or brittle nails. Blood tests, specifically the complete blood count (CBC), are standard diagnostic tools [4]. This common diagnostic test evaluates multiple blood constituents, such as red blood cells, white blood cells, and platelets. A primary factor in distinguishing between anemic and non-anemic individuals is the blood's hemoglobin level, which is quantified in grams per deciliter (g/dL) [5]. The WHO establishes a common hemoglobin threshold of 11 g/dL, though this value can vary based on factors such as age, sex, and geographical location [1].

Non-invasive methods for detecting anemia, relying on the processing and analysis of images from specific body regions, have become a prominent area of research in recent years. A predictive relationship exists between changes in cutaneomucosal pallor and the presence of anemia [6]. Generally, the visible characteristics associated with anemia and the signs of pallor assessed in non-invasive detection methods include the palmar region, the nail beds, and the ocular conjunctiva [5] (see Figure 1). While significant progress has been made in anemia detection through conjunctival image analysis, most previous studies have been confined to controlled environments with artificial lighting [7]. However, in outdoor settings, variability in natural illumination introduces challenges that affect image quality and, consequently, the accuracy of segmentation and classification algorithms [8]. Typically, efforts to address variations in contrast and coloration in ocular conjunctival images involve calibration using standard color tables [9]. However, this approach not only requires complex automation to identify the color region of interest (captured simultaneously with the conjunctival region in the photograph) and calibrate the images within the dataset but has also proven to be ineffective in environments with uncontrolled lighting conditions [7]. Other studies explore various image enhancement techniques to counteract the effects of lighting variations in conjunctival images for non-invasive anemia detection. Among these, Contrast-Limited Adaptive Histogram Equalization (CLAHE) has been widely used for feature enhancement and detail detection in medical images [10]. More recently, the Retinex algorithm [11] has gained attention due to its ability to enhance image contrast while preserving

natural color appearance. Retinex, inspired by human visual perception, corrects illumination inconsistencies by estimating the reflectance of an image, making it particularly effective in low-contrast conditions.

This study addresses this gap by proposing a novel preprocessing pipeline specifically designed for conjunctival images captured outdoors. Our method, which combines grayscale histogram normalization, LAB color space-based artifact inpainting, and adaptive contrast enhancement, effectively mitigates the effects of uneven illumination, glare, and reflections. To our knowledge, this is the first pipeline dedicated to improving the quality of conjunctival images acquired in uncontrolled environments for anemia detection.

Fig. 1. Photograph of the ocular conjunctiva

2 MATERIALS AND METHODS

2.1 Dataset collection

A number of publicly available datasets in scientific and medical article repositories contain categorized images of various ocular surface tissues. These datasets specifically include images of the palpebral, forniceal, and scleral regions of the conjunctiva. Previous studies focusing on non-invasive anemia detection [8] have frequently utilized the following open-access databases:

EYES-DEFY-ANEMIA Dataset: The Eyes-Defy-Anemia Dataset [12] comprises 218 eye images, specifically segmented and unsegmented conjunctival images, which can be utilized to investigate the diagnosis or estimation of anemia based on the pallor of the human ocular conjunctiva. These images are also valuable for the study of segmentation algorithms for the conjunctiva or the exposed portions of the sclera and iris. All images in the dataset are accompanied by segmented elements (palpebral and forniceal conjunctiva), which is valuable both for directly correlating pallor with hemoglobin (Hb) concentration levels and for evaluating the performance of segmentation algorithms. Furthermore, each image includes relevant information such as the lab-measured hemoglobin value, patient age, and sex. The images were captured with a Samsung S6 smartphone, equipped with a capture device that magnifies the images, standardizes lighting, and eliminates the influence of ambient light. Consequently, all images were taken at the same distance and with uniform lighting based on white LED light. The segmentation of the eye areas was performed by trained personnel based on their own interpretation [7].

CP-AnemiC Dataset from Ghana: The authors [8] present a dataset focused on the evaluation of conjunctival pallor area related to hemoglobin concentration levels in 710 patients, motivated by the scarcity of open-access datasets available related to this topic. Data collection was carried out in various regions of Ghana in patients

aged between 6 and 59 months. The dataset includes color images segmented in the region of interest, along with additional information linked to each sample, such as hemoglobin concentration levels, age, gender, and city of origin. Furthermore, the World Health Organization (WHO) classification criteria for the detection of anemia in children were followed, where anemia is considered when the hemoglobin level is less than 11 g/dL, and non-anemia when it is greater than or equal to 11 g/dL. To protect patient privacy, the dataset does not include unsegmented conjunctival photographs. The photographs were captured with a simple 12-megapixel camera in an outdoor environment, with natural lighting and without the use of flash or artificial lights [8]. Employing images pre-labeled as 'anemic' or 'non-anemic' by the dataset authors for binary classification, this study proceeded independently of the provided hemoglobin level information (see Table 1).

Table 1. Characteristics of the EYES-DEFY-ANEMIA and CP-AnemiC Datasets

Characteristic	EYES-DEFY-ANEMIA [12]	CP-AnemiC [8]
Number of images	218	710
Available photograph	Yes	No
Available segmentation	Yes	Yes
Segmentation type	Manual	Manual
Image format	PNG	JPG
Capture device	Samsung S6 16-megapixels	12-megapixels camera
Patient age range	18–53 years	6–59 months
Lighting condition	Indoor (Natural, white LED Lighting)	Outdoor (Natural, No Flash)
Anemia criterion	Not specified	<11 g/dL
Location	India, Italy	Ghana
Preprocessing	Not present	Not present
Region of Interest	Palpebral conjunctiva	Palpebral conjunctiva, palms and nails
Data Augmentation	No	No

The partitioning of the subsets was performed as follows: 70% of the images from each class were assigned to the "training" subset, 15% to the "validation" subset, and the remaining 15% to the "test" subset. To ensure rigorous control over the distribution, the splits were performed according to the alphabetical order of the image filenames. This approach ensures that the number of images and the representation of each class are consistent across the datasets, both with and without preprocessing. This allows for a reproducible evaluation of the performance of the segmentation and classification models.

2.2 Proposed processing

To mitigate the impact of luminance variations in conjunctival images acquired in uncontrolled or outdoor environments, we designed and implemented a comprehensive image preprocessing pipeline. This pipeline is a key component of our methodology for non-invasive anemia detection, which comprises three main phases: (1) Preprocessing: Our proposed pipeline, detailed in Figure 2, employs a sequential combination of grayscale normalization, artifact inpainting using the LAB color space, and adaptive contrast enhancement to address issues stemming from uncontrolled

ambient lighting, such as glare and uneven illumination. (2) Segmentation: Following preprocessing, the enhanced images undergo automatic segmentation of the ocular conjunctiva using deep learning models. (3) Classification: Finally, the segmented conjunctiva regions are classified as anemic or non-anemic using state-of-the-art methods. The effectiveness of our preprocessing pipeline will be validated through the expected improvement in segmentation and classification metrics.

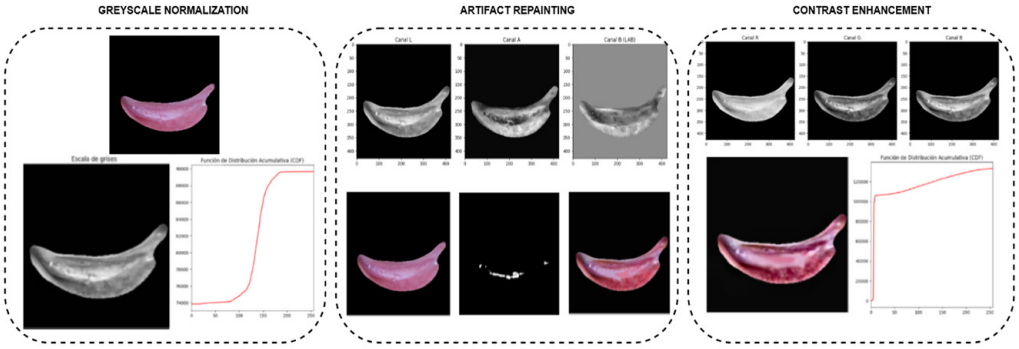

Fig. 2. Diagram of the proposed light variability correction preprocessing pipeline

Grayscale Histogram Normalization: To homogenize brightness and contrast across the images, histogram normalization is applied. This technique adjusts the distribution of intensity (luminosity) values, improving image uniformity and highlighting critical details [13].

The first step involves loading the image in a format that facilitates the analysis of its intensity levels. This is achieved by converting the original RGB image to grayscale, where each pixel is represented by a value in the range of 0 to 255, corresponding to the intensity of gray [14]. Equation 1 defines the transformation from the original RGB image to its corresponding grayscale representation, which is fundamental for subsequent histogram normalization.

$$I_{gray} = 0.2989 \cdot R + 0.5870 \cdot G + 0.1140 \cdot B \quad (1)$$

This transformation is crucial for simplifying processing by reducing the complexity of the information to a single intensity channel. Once the image is loaded, its histogram is calculated. The histogram is a graphical representation showing the distribution of intensity values within the image. A vector of 256 elements is created, where each index represents an intensity level, and the value at each index indicates the number of pixels with that intensity [15]. This step is crucial to observe the luminosity distribution and to identify low-contrast areas in the original image.

The Cumulative Distribution Function (CDF) is computed from the histogram and represents the cumulative probability of intensity levels [16]. This step involves an accumulated sum of the histogram values. The CDF is normalized by dividing each element by the maximum CDF value, ensuring the values are in the range (0, 1). This step is essential to adjust the intensity values proportionally to the original distribution. The normalization is performed by applying the CDF to the original intensity values of the image. This process involves mapping each intensity value to a new value using linear interpolation. By multiplying the normalized CDF by 255, the new values are ensured to be within the proper range for a grayscale image. The resulting image shows a better distribution of gray levels, improving overall brightness and highlighting features that may have previously been difficult to observe.

Reflection Removal by Artifacts Inpainting: The objective is to restore areas that may represent flashes or excessive brightness without significantly altering the visual context of the image. This process ensures that the subsequent analysis or use of the images is not affected by unwanted luminous artifacts [17]. The proposed reflection removal process is described below: The first step in reflection removal is to convert the normalized image from the BGR color space to the LAB color space. The LAB space is more suitable for detecting luminance ('L' channel), separating luminosity information from chromatic information. This is useful because reflections often appear as peaks in luminosity, and the L channel allows a direct identification of these areas. A thresholding technique is used on the L channel to detect areas with intense brightness. This threshold (*light_treshhold* = 220) identifies pixels that exceed a certain luminosity value and considers them affected by reflections. The output is a binary mask (0 or 255) where pixels with values above the threshold are marked as 255, representing the bright zones. Then, a dilation operation using a 3×3 kernel is used to expand the detected bright areas [18]. This ensures that any nearby region affected by reflections is included in the mask. To avoid painting over black areas or areas outside the area of interest, another mask is created to identify completely black pixels, using a low threshold. The restoration process is guided by Equation 2.

$$I_{inpaint}(x,y) = \frac{\sum_{(i,j)\in N(x,y)} w_{ij} \cdot I(i,j)}{\sum_{(i,j)\in N(x,y)} w_{ij}} \quad (2)$$

The final artifact mask is obtained by combining the bright areas mask while excluding the black areas. This ensures action is taken only on bright zones that are not part of the black background or other non-relevant areas. The areas marked in the artifact mask are repainted using a weighted average of neighboring non-local pixels. For each bright pixel, a neighborhood (18×18 pixels around it) is taken, and the average value of non-bright neighbor pixels is calculated [19]. The closer the neighboring pixels, the higher their weight in the average, as shown in Figure 3.

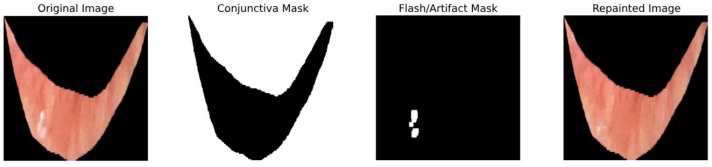

Fig. 3. Reflection detection and repainting on segmented conjunctiva

Adaptive Contrast Enhancement: Contrast Limited Adaptive Histogram Equalization (CLAHE) technique is used to mitigate the effects of light variability in each RGB color channel. CLAHE is a variant of histogram equalization where the image is divided into smaller regions (tiles or blocks), and histogram equalization is applied locally to each region. This avoids over-enhancement in low-contrast areas, where global equalization may lead to the amplification of noise or the loss of detail [20].

After detecting the flashes, the preprocessing for the light variability correction resumes on the conjunctiva images in the following way: For each RGB channel of the image, the intensity histogram is calculated. The histogram has 256 bins (grayscale levels), with intensity values between 0 and 255. The *clip_limit* parameter that defines the threshold that limits the maximum height of the histogram is set to 2.0. This prevents the excessive amplification of contrast in high-brightness or shadow areas. The limit is calculated based on the average of the histogram and

the tile size defined, divided into an 8×8 grid of blocks. Subsequently, the CDF of the limited histogram is calculated (Equation 3). This process redistributes the intensity values to enhance the contrast in each tile.

$$CDF_{local}(i) = \frac{\sum_{j=0}^{i} H_{local}(j)}{N_{local}} \tag{3}$$

The CDF normalization is performed to ensure values are in the range of 0 to 255 [21]. The normalized CDF is applied to the image's intensity values in the corresponding channel, enhancing local contrast without amplifying noise (Equation 4). Once the algorithm is applied to each of the RGB channels, these channels are recombined to obtain the final image. This process ensures that local contrast has been optimized for all channels of the conjunctiva image. By appropriately combining the channels, color fidelity is preserved while maintaining enhanced contrast.

$$I_{CLAHE}(x, y) = 255 \cdot \frac{CDF_{local}(I(x, y))}{max(CDF_{local})} \tag{4}$$

Finally, after processing the ocular conjunctiva images using these three methods, the resulting images exhibit enhanced details, as illustrated in Figure 4.

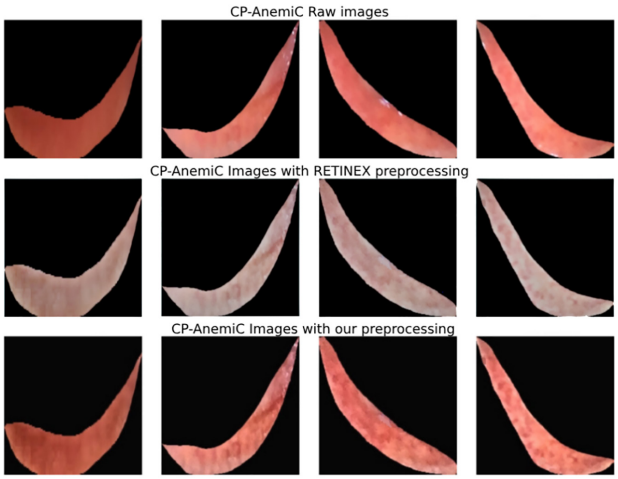

Fig. 4. Before and after the application of the proposed processing

2.3 Segmentation models

The study employed three distinct convolutional neural network architectures for image segmentation: BiSeNet [21], U-Net [22], and ConjunctiveNet [23]. To ensure a fair and unbiased comparison of their performance on the dataset, both with and without the proposed preprocessing, models were trained using the fixed hyperparameters detailed in Table 2 and selected using the GridSearch technique [24]. These models were trained with an input size of 256×256 RGB images, utilizing ReLU activation functions in their intermediate layers and a sigmoid function in the output layer, appropriate for binary segmentation [22]. The training process for the networks was driven by the Adam optimizer, with a learning rate of 1e-4 and the Dice loss function, incorporating a smoothing factor of 1e-6. Furthermore, training was conducted with a batch size of 32 over 20 epochs. While BiSeNet, designed for real-time segmentation,

demonstrated efficient processing with faster inference times, U-Net excelled in preserving finer details in complex structures, attributed to its encoder-decoder architecture with skip connections [25]. On the other hand, ConjunctiveNet is a method specifically designed for the automatic segmentation of the conjunctiva. It employs a preprocessing approach based on CLAHE to enhance the sampling of the region of interest. The segmentation is performed using convolutional neural networks (CNNs) with transfer learning techniques, further refined through a modified Otsu method [23].

Maintaining these hyperparameters constant across all experimental conditions allowed for a direct evaluation of the impact of the proposed preprocessing method on segmentation performance (see Table 2).

Table 2. Hyperparameters of semantic segmentation models

Hyperparameter	BiSeNet [21]	U-Net [22]	ConjunctiveNet [23]
Input size	(256, 256, 3)	(256, 256, 3)	(256, 256, 3)
Intermediate layers activation function	ReLU	ReLU	ReLU
Output layer activation function	Sigmoid	Sigmoid	Softmax
Loss function	DiceLoss (smoothing 1e-6)	DiceLoss (smoothing 1e-6)	DiceLoss (smoothing 1e-6)
Optimizer	Adam	Adam	Adam
Learning rate	1e-4	1e-4	1e-4
Batch size	32	32	32
Epochs	20	20	20

2.4 Classification models

ANN Model: The classification task was performed using a fully connected, feed-forward artificial neural network (ANN). The network comprised three dense layers with 100, 50, and 1 neuron, respectively. ReLU activation functions were applied to the intermediate layers, while the output layer used a sigmoid activation function, which is standard for binary classification problems. The network was trained to minimize the binary cross-entropy loss using the Adam optimizer, and the training process used a batch size of 32 and a total of 1000 epochs, which allowed the model to effectively converge and learn the underlying patterns in the data. Among the evaluated features were the mean and standard deviation of RGB and LAB color channel values, along with brightness intensity, luminance, homogeneity, entropy, texture, and other relevant characteristics for the detection of anemia through variations in clinical pallor of the human ocular conjunctiva, suggested by [7]. Furthermore, no early stopping, adaptive batch size, or other training modification techniques were employed to ensure replicability.

CNN-ResNet: ResNet (residual network) is a CNN architecture designed to address the vanishing gradient problem in deep networks. The key innovation of ResNet lies in the introduction of residual blocks, which enable information flow through skip connections. These connections bypass one or more layers and add the original input to the output of the convolutional layers, facilitating the training of extremely deep networks by mitigating gradient degradation. This structure allows the network to learn residual functions rather than complete functions, simplifying optimization and enhancing performance in computer vision tasks. ResNet has proven effective in

applications such as image classification, object detection, and segmentation, thanks to its ability to train networks with dozens or even hundreds of layers without losing accuracy. For our classification task, ResNet-50 (a variant with 50 layers) is used as a base model for transfer learning, leveraging its capability to extract hierarchical features from RGB images of size (256, 256, 3). The architecture employs ReLU activation functions in intermediate layers and a sigmoid activation in the output layer, optimized using Binary Crossentropy and the Adam algorithm with a learning rate of 0.001. This approach enables efficient and accurate classification, particularly in tasks where network depth is crucial for capturing complex data patterns [26].

SLIC-GAT: This method [9] is an approach based on image processing and graph attention networks (GAT) for the non-invasive estimation of hemoglobin levels from digital images of the palpebral conjunctiva. The process begins with image segmentation into superpixels using the SLIC (simple linear iterative clustering) algorithm, which groups pixels into homogeneous regions based on color similarity (LAB color space) and spatial proximity. For each superpixel, statistical descriptors such as the standard deviation (σL, σa), mode (ML, Ma) of the L and a color channels, and the average spatial coordinates (μx, μy) are extracted. These descriptors are organized into a graph structure, where nodes represent superpixels and edges connect adjacent nodes. The SLIC-GAT model employs graph attention layers (GAT) to process this structure, enabling the model to learn spatial and feature relationships among superpixels. Finally, a fully connected neural network (MLP) takes the features processed by the GAT layers and performs regression to estimate hemoglobin levels. The model is trained by minimizing the mean squared error (MSE) between predictions and actual hemoglobin values. This approach combines advanced image processing techniques, graph-based machine learning, and regression, making it a promising tool for anemia detection in low-resource settings [9].

Each model developed for the classification task of anemia detection using segmented conjunctival images was trained using the parameters specified in Table 3. These parameters were optimized through a GridSearch [24] approach, keeping the learning rate and batch size fixed to determine the optimal minimum number of epochs, tailored to the specific requirements of the problem.

Table 3. Hyperparameters of methods for anemia classification

Hyperparameter	ANN [7]	CNN-ResNet [26]	SLIC-GAT [9]
Network architecture	3 dense layers (100, 50, 1 neurons)	Transfer Learning ResNet-34	GAT layers + MLP (32, 32, 1 neurons)
Input image size	(256, 256, 3)	(256, 256, 3)	20 Superpixel Segments
Intermediate layers activation function	ReLU	ReLU	ReLU
Output layer activation function	Sigmoid	Sigmoid	Linear
Loss function	Binary Crossentropy	Binary Crossentropy	Sigmoid
Optimizer	Adam	Adam	Adam
Learning rate	0.005	0.001	0.001
Batch size	32	32	32
Epochs	1000	100	100
Input data	21 extracted features	RGB Images	Statistical descriptors of segments

3 RESULTS

3.1 Evaluation metrics

The purpose of model evaluation is to validate that the patterns learned from the training data can be successfully applied to a separate validation or testing dataset. Based on the study by Branco et al. [27], we adopted the ensuing performance metrics:

Accuracy: Accuracy measures the proportion of correct predictions made by the model relative to the total number of predictions. For pixel-level segmentation, accuracy quantifies the proportion of correctly classified pixels across the entire image.

$$accuracy = \frac{TP + TN}{TP + TN + FP + FN} \tag{5}$$

Precision: Calculates the proportion of true positive predictions among all positive predictions. This metric is critical in applications where the cost of false positives is high, requiring high reliability in identifying positive cases. For segmentation, precision represents the ratio of correctly classified positive pixels to the total predicted positive pixels.

$$precision = \frac{TP}{TP + FP} \tag{6}$$

Recall: also known as sensitivity or true positive rate, measures the proportion of actual positive cases correctly identified by the model. It is vital in scenarios where minimizing false negatives is essential, as in applications with consequences for missed detections. In segmentation tasks, recall quantifies how well the model captures all the pixels belonging to the positive class.

$$recall = \frac{TP}{TP + FN} \tag{7}$$

F1-score: By computing the harmonic mean of precision and recall, the F1-score provides a single performance metric that accounts for both false positives and false negatives. It proves especially advantageous when dealing with imbalanced datasets, necessitating a balance between precision and recall for effective evaluation. For segmentation, the F1-score assesses the overlap between the predicted and ground-truth positive pixels, balancing under-segmentation and over-segmentation.

$$F1\text{-}score = \frac{2 \cdot precision \cdot recall}{precision + recall} \tag{8}$$

Intersection over Union (IoU): or Jaccard Index, measures the overlap between predicted and actual regions, serving as a critical performance metric for segmentation. It evaluates the pixel-level agreement between predicted segmentations and the ground truth [28].

$$IoU = \frac{A_{predicted} \cap A_{real}}{A_{predicted} \cup A_{real}} \tag{9}$$

Dice Coefficient: The Dice Similarity Coefficient (DSC) is a statistical metric used to evaluate the similarity between two sets, commonly applied in image

segmentation tasks to measure the overlap between a predicted segmentation and the ground truth. It is particularly useful for imbalanced datasets, as it emphasizes agreement while mitigating the impact of class imbalance [29].

$$Dice = \frac{2 \cdot \left| A_{predicted} \cap A_{real} \right|}{\left| A_{predicted} \right| + \left| A_{real} \right|} \tag{10}$$

3.2 Segmentation results

The segmentation process using BiSeNet, configured with the parameters outlined in Table 2, is illustrated in the samples shown in Figure 5. In this process, the predicted mask is initially represented in continuous grayscale values ranging from 0 to 255. Subsequently, a binary mask is generated by applying a midpoint threshold. Specifically, all pixel values in the Predicted Mask greater than or equal to 128 are set to 255 (white), while those below 128 are set to 0 (black). This binarized mask is then utilized for automated segmentation and performance evaluation. The evaluation was performed on the test subset, and we deliberately avoided data augmentation to ensure the replicability of the experimental results.

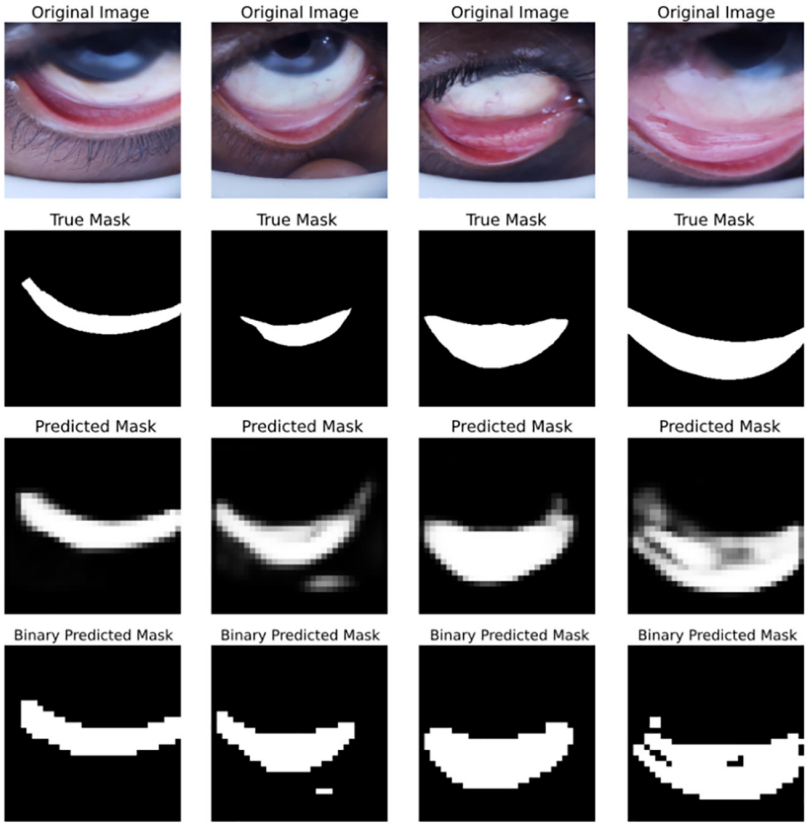

Fig. 5. Segmented binary mask outputs generated by the BiSeNet architecture

Similarly, Figure 6 illustrates the prediction of automatically segmented masks generated using the U-Net-based model architecture compared to the masks provided by the Eyes-defy-anemia dataset, which serve as ground truth. The predicted masks and their corresponding metrics were obtained during the evaluation of the test data subset, without data augmentation. Also observed in Figure 7 is the behavior

of automatic mask estimation of the resulting model using the ConjuntiveNet methodology and architecture under the same conditions.

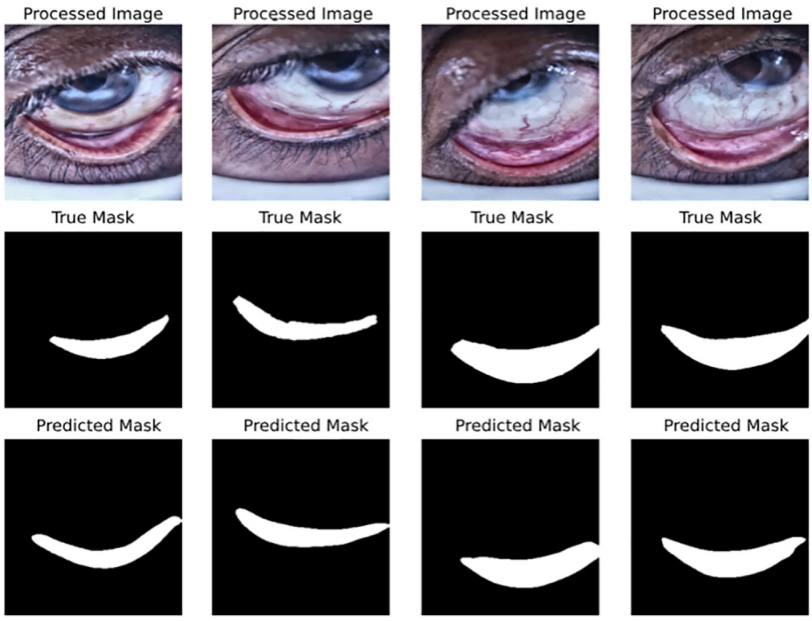

Fig. 6. Segmented binary mask outputs generated by the U-Net architecture

Table 4 shows the performance of the BiSeNet, U-Net, and ConjunctiveNet segmentation architectures on the Eyes-defy-anemia India dataset, evaluated under varying lighting conditions. For each architecture, 10 independent trials (models) were run, and the standard deviation of each metric was calculated. A comparative analysis is also included, incorporating images processed with the well-established RETINEX algorithm [11], as illustrated in Figure 4. RETINEX has been widely applied in uncontrolled lighting environments to enhance image contrast and improve automatic classification metrics [30]. In Table 4, we evaluate its performance against our proposed preprocessing pipeline in semantic segmentation tasks.

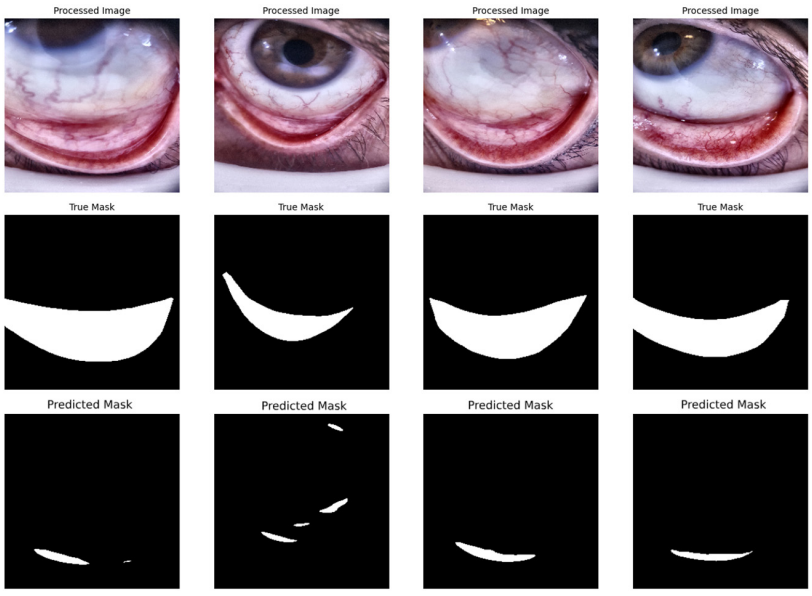

Fig. 7. Segmented binary mask outputs generated by the ConjunctiveNet architecture

Table 4. Segmentation model results on the Eyes-Defy-Anemia Dataset with and without preprocessing

Metric	BiSeNet			U-Net			ConjunctiveNet		
	Without Processing	With RETINEX	With Our Processing	Without Processing	With RETINEX	With Our Processing	Without Processing	With RETINEX	With Our Processing
Accuracy	94.02 ± 0.48	85.31 ± 1.19	94.74 ± 0.28	95.87 ± 0.69	93.92 ± 1.19	96.13 ± 0.47	87.87 ± 1.19	89.02 ± 1.19	91.13 ± 0.47
Precision	71.38 ± 5.16	74.31 ± 4.63	80.34 ± 4.14	80.08 ± 5.63	82.83 ± 3.01	84.22 ± 2.38	79.18 ± 3.22	82.31 ± 3.29	84.82 ± 2.01
Recall	90.20 ± 7.10	77.45 ± 7.19	78.31 ± 7.49	90.07 ± 4.00	83.27 ± 3.14	84.79 ± 3.67	86.13 ± 3.10	81.10 ± 5.23	85.79 ± 3.67
F1-score	79.24 ± 0.71	75.85 ± 5.37	78.87 ± 2.57	84.51 ± 1.68	83.05 ± 1.59	84.54 ± 2.05	84.61 ± 2.76	81.61 ± 1.77	87.44 ± 2.05
IoU	65.63 ± 0.98	64.22 ± 2.19	65.19 ± 3.41	73.21 ± 2.51	73.13 ± 2.19	73.91 ± 3.01	75.63 ± 1.91	71.27 ± 1.57	74.33 ± 3.01
Dice Coefficient	79.25 ± 0.72	78.23 ± 1.62	78.9 ± 2.50	84.47 ± 1.67	84.40 ± 0.98	84.59 ± 2.03	84.52 ± 1.37	84.53 ± 1.06	85.86 ± 2.05

3.3 Classification results

The anemia classification results on the test subset, obtained using the proposed artificial neural network models based on feature extraction, are presented in Table 5. These results are reported for both the CP-AnemiC Ghana dataset and the Eyes-Defy-Anemia India Dataset, using a hemoglobin cutoff of 11 g/dL for classification [7] and comparing the performance of images and their predictions before and after applying the proposed preprocessing method. All datasets were processed using models built under the best parameters found for the smallest number of epochs considering the same batch size, defined by the GridSearch algorithm (refer to Table 3). Across 10 evaluation iterations, the proposed method consistently improved metric outcomes.

Table 5. Classification results using classification models on conjunctival datasets

Metric	CP-AnemiC			Eyes-Defy-Anemia		
	Without processing	With RETINEX	With our processing	Without processing	With RETINEX	With our processing
ANN, Dimauro et al. [7]						
Accuracy	81.54 ± 1.77	82.12 ± 1.89	85.51 ± 1.40	85.94 ± 2.71	83.14 ± 1.99	88.28 ± 2.59
Precision	87.35 ± 1.37	84.03 ± 2.11	91.44 ± 2.84	77.24 ± 3.16	81.27 ± 2.79	83.57 ± 2.62
Recall	80.86 ± 2.31	78.18 ± 2.43	81.64 ± 2.56	95.43 ± 3.57	87.38 ± 3.91	92.86 ± 5.05
F1-score	81.91 ± 1.53	81.00 ± 1.99	85.08 ± 1.12	85.73 ± 2.68	84.21 ± 2.93	87.35 ± 2.99
CNN-ResNet, Purwanti et al. [26]						
Accuracy	81.54 ± 1.77	82.70 ± 1.89	86.76 ± 1.70	87.94 ± 2.13	86.07 ± 2.89	89.17 ± 1.79
Precision	87.35 ± 1.37	87.94 ± 1.97	92.14 ± 1.54	81.24 ± 2.74	82.09 ± 1.45	87.57 ± 2.82
Recall	80.86 ± 2.31	81.59 ± 1.89	86.34 ± 2.39	89.43 ± 3.01	87.70 ± 3.13	93.86 ± 2.12
F1-score	81.91 ± 1.53	84.65 ± 1.61	89.15 ± 1.96	85.14 ± 2.38	84.80 ± 1.99	90.61 ± 1.94
SLIC-GAT, Moreno et al. [9]						
Accuracy	80.26 ± 2.19	71.35 ± 2.03	82.51 ± 1.67	84.64 ± 2.11	73.81 ± 2.51	86.17 ± 1.69
Precision	66.45 ± 1.97	64.22 ± 1.49	83.07 ± 1.85	81.24 ± 3.12	69.36 ± 2.41	84.49 ± 2.02
Recall	69.81 ± 2.27	70.33 ± 2.07	83.76 ± 0.93	86.93 ± 2.43	74.38 ± 1.87	88.36 ± 3.15
F1-score	68.09 ± 2.20	67.12 ± 1.85	83.41 ± 1.24	83.99 ± 2.37	71.78 ± 2.14	86.38 ± 2.70

4 DISCUSSION

4.1 Analysis of segmentation results

The segmentation performance of conjunctival images was assessed using three semantic segmentation models—BiSeNet, U-Net, and ConjunctiveNet—under three conditions: no preprocessing, RETINEX preprocessing, and the proposed processing method. The results, summarized from Table 4, demonstrate that the proposed method enhances key metrics such as precision and accuracy across all models, though its impact varies depending on the model and specific metric.

The proposed method markedly improved precision from 71.38% to 80.34%, outperforming RETINEX's 74.31%, which suggests a significant reduction in false positives. Accuracy also increased from 94.02% to 94.74%, surpassing RETINEX's 85.31%. The Dice Coefficient rose from 79.25% to 84.47%, indicating greater segmentation similarity. However, recall decreased from 90.20% to 78.31%, and the F1-score slightly declined from 79.24% to 78.87%, with IoU dropping from 65.63% to 65.19%. These results indicate that the method prioritizes precision and accuracy, with some trade-offs in recall and overlap metrics.

For U-Net, the proposed method yielded consistent improvements across multiple metrics. Accuracy increased from 95.87% to 96.13%, exceeding RETINEX's 93.92%. Precision improved from 80.08% to 84.22% (compared to 82.83% with RETINEX), while recall decreased from 90.07% to 84.79%. The F1-score saw a marginal increase from 84.51% to 84.54%, IoU advanced from 73.21% to 75.91%, and the Dice Coefficient rose from 84.47% to 85.86%. These gains underscore the method's ability to enhance segmentation quality in U-Net, balancing precision improvements with better overlap metrics.

In ConjunctiveNet, accuracy improved from 87.87% to 91.13%, outperforming RETINEX's 89.02%. Precision increased from 79.18% to 84.22% (vs. 82.31% with RETINEX), while recall dropped from 88.13% to 84.79%. The Dice Coefficient advanced from 84.52% to 85.86%, reflecting improved segmentation similarity. However, the F1-score slightly decreased from 84.61% to 84.54%, and IoU declined from 75.63% to 74.33%. These mixed outcomes suggest gains in precision and accuracy, with minor reductions in F1-score and IoU.

Across the models, U-Net and ConjunctiveNet outperformed BiSeNet in precision, IoU, and Dice Coefficient under the proposed method. Precision improvements over RETINEX were 6.03% for BiSeNet (80.34% vs. 74.31%), 1.39% for U-Net (84.22% vs. 82.83%), and 1.91% for ConjunctiveNet (84.22% vs. 82.31%). U-Net exhibited the most consistent enhancements, with gains in accuracy, F1-score, IoU, and Dice Coefficient, making it the strongest performer. ConjunctiveNet improved in precision, accuracy, and Dice Coefficient, though with slight declines in F1-score and IoU. BiSeNet showed notable precision and accuracy gains but had minor reductions in F1-score and IoU, indicating a more limited overall benefit.

Despite a consistent reduction in recall across all models, the proposed method effectively reduces false positives and enhances segmentation reliability, as evidenced by improved precision and Dice Coefficient values, particularly in U-Net and ConjunctiveNet. These findings highlight the method's potential to improve segmentation quality, with the most pronounced benefits observed in high-performing models like U-Net.

4.2 Analysis of classification results

Table 5 presents the evaluation of three semantic segmentation techniques—ANN, CNN-ResNet, and SLIC-GAT—for conjunctival segmentation, conducted on the CP-AnemiC and Eyes-defy-anemia datasets, and demonstrates that our proposed processing method significantly enhances performance compared to unprocessed images and those preprocessed with RETINEX. For the ANN model, our processing method markedly improved performance. On the CP-AnemiC dataset, accuracy increased from 81.54% (unprocessed) and 82.12% (RETINEX) to 85.51%, while precision rose from 87.35% and 84.03% to 91.44%, reflecting a stronger capacity to identify true positives. On the Eyes-defy-anemia dataset, accuracy improved from 85.94% to 88.28%, precision from 77.24% to 83.57%, and the F1-score from 85.73% to 87.35%. These results highlight the superiority of our method over RETINEX, which produced inconsistent gains, thus affirming its effectiveness in optimizing conjunctival segmentation.

The CNN-ResNet model also exhibited substantial benefits. On the CP-AnemiC dataset, accuracy rose from 81.54% (unprocessed) and 82.70% (RETINEX) to 86.76%, with precision climbing from 87.35% to 92.14% and the F1-score from 81.91% to 89.15%. On the Eyes-defy-anemia dataset, accuracy increased from 87.94% to 89.17%, precision from 81.24% to 87.57%, and the F1-score from 85.14% to 90.61%. These consistent improvements demonstrate that our method not only outperforms RETINEX but also enhances both precision and recall concurrently.

The SLIC-GAT model showed the most pronounced enhancements with our processing method. On the CP-AnemiC dataset, accuracy improved from 80.26% (unprocessed) and 71.35% (RETINEX) to 82.51%, while precision surged from 66.45% to 83.07% and the F1-score from 68.09% to 83.41%, reversing the performance decline observed with RETINEX. On the Eyes-defy-anemia dataset, accuracy rose from 84.64% to 86.17%, precision from 81.24% to 84.49%, and the F1-score from 83.99% to 86.38%. These results underscore our method's ability to overcome RETINEX's limitations, delivering substantial and reliable performance gains.

5 CONCLUSIONS

In this study, we developed an innovative preprocessing pipeline tailored for conjunctival images captured in uncontrolled outdoor environments. This pipeline integrates grayscale histogram normalization, LAB color space-based artifact inpainting, and adaptive contrast enhancement to effectively address illumination variability. Our results demonstrate that this method consistently outperforms both unprocessed images and those preprocessed with the RETINEX method across segmentation and classification tasks for non-invasive anemia detection.

For segmentation, the proposed pipeline significantly enhanced precision across all evaluated models: BiSeNet, U-Net, and ConjunctiveNet. Specifically, U-Net achieved a precision increase from 80.08% to 84.22%, surpassing RETINEX (82.83%) by 1.39%, while ConjunctiveNet improved from 79.18% to 84.22%, exceeding RETINEX (82.31%) by 1.91%. BiSeNet exhibited a notable precision gain from 71.38% to 80.34%, outperforming RETINEX (74.31%) by 6.03%. Despite a consistent reduction in recall across all models (e.g., U-Net: 90.07% to 84.79%; ConjunctiveNet: 88.13% to 84.79%; BiSeNet: 90.20% to 78.31%), the overall segmentation quality improved, particularly for U-Net, as evidenced by gains in F1-score (84.51% to 84.54%), IoU

(73.21% to 75.91%), and Dice Coefficient (84.47% to 85.86%). ConjunctiveNet showed a mixed outcome with an improved Dice Coefficient (84.52% to 85.86%) but slight declines in F1-score (84.61% to 84.54%) and IoU (75.63% to 74.33%). These findings highlight the method's ability to reduce false positives and enhance segmentation reliability under challenging lighting conditions, with U-Net demonstrating the most consistent improvements.

In the classification task, our preprocessing approach significantly elevated performance across ANN, CNN-ResNet, and SLIC-GAT models on the CP-AnemiC (Ghana) and Eyes-defy-anemia (India) datasets. For ANN, accuracy on the Ghana dataset increased by 3.97% from 81.54% to 85.51%, with precision rising from 87.35% to 91.44%, while on the India dataset, accuracy improved by 2.34% from 85.94% to 88.28%, with precision advancing from 77.24% to 83.57%. CNN-ResNet achieved accuracy gains to 86.76% (Ghana) and 89.17% (India), with precision reaching 92.14% and 87.57%, respectively. SLIC-GAT exhibited the most substantial enhancement, reversing RETINEX's performance decline (e.g., accuracy drop from 80.26% to 71.35% on Ghana) and achieving a precision increase from 66.45% to 83.07% on the Ghana dataset, alongside accuracy improvements to 82.51% (Ghana) and 86.17% (India). These results underscore the proposed method's superiority over RETINEX, which demonstrated inconsistent or diminished gains, affirming its robustness in optimizing feature extraction and classification accuracy.

This work addresses a critical gap by enabling reliable processing of conjunctival images under variable natural lighting, a challenge that has limited prior studies focused on controlled environments. The proposed pipeline offers a robust solution for real-world anemia detection, with potential for integration into portable diagnostic tools to enhance accessibility in resource-limited settings. Future research could refine this approach by optimizing the precision-recall trade-off through techniques such as dynamic thresholding and by expanding dataset diversity to encompass broader environmental conditions. Additionally, the method's adaptability suggests applicability to other pallor-based conditions or ocular diagnostics, potentially broadening its impact in telemedicine and field healthcare.

6 REFERENCES

[1] World Health Organization, "Anaemia," 2023. [Online]. Available: https://www.who.int/es/news-room/fact-sheets/detail/anaemia. [Accessed: 2023].

[2] G. A. Stevens *et al.*, "National, regional, and global estimates of anaemia by severity in women and children for 2000–19: A pooled analysis of population-representative data," *The Lancet Glob. Heal.*, vol. 10, no. 5, pp. e627–e639, 2022. https://doi.org/10.1016/S2214-109X(22)00084-5

[3] A. D. C. Ochoa Salazar, "Valor predictivo de la palidez cutaneomucosa en el diagnostico de anemia en niños de 6 meses a 60 meses atendidos en el centro de salud Jesús Poderoso de San Juan de Miraflores – Lima durante el año 2020," Universidad Privada San Juan Bautista, 2021.

[4] S. S. Abdul-Jabbar, A. K. Farhan, and A. S. Luchinin, "A comparative study of anemia classification algorithms for international and newly CBC datasets," *International Journal of Online and Biomedical Engineering (iJOE),* vol. 19, no. 6, pp. 141–157, 2023. https://doi.org/10.3991/ijoe.v19i06.38157

[5] C. Camaschella and D. Girelli, "The changing landscape of iron deficiency," *Mol. Aspects Med.*, vol. 75, p. 100861, 2020. https://doi.org/10.1016/j.mam.2020.100861

[6] S. Mahmud, T. B. Donmez, M. Mansour, M. Kutlu, and C. Freeman, "Anemia detection through non-invasive analysis of lip mucosa images," *Front. Big Data*, vol. 6, 2023. https://doi.org/10.3389/fdata.2023.1241899

[7] J. W. Asare, P. Appiahene, E. T. Donkoh, and G. Dimauro, "Iron deficiency anemia detection using machine learning models: A comparative study of fingernails, palm and conjunctiva of the eye images," *Engineering Reports*, vol. 5, no. 11, p. e12667, 2023. https://doi.org/10.1002/eng2.12667

[8] P. Appiahene, K. Chaturvedi, J. W. Asare, E. T. Donkoh, and M. Prasad, "CP-AnemiC: A conjunctival pallor dataset and benchmark for anemia detection in children," *Medicine in Novel Technology and Devices*, vol. 18, p. 100244, 2023. https://doi.org/10.1016/j.medntd.2023.100244

[9] G. Moreno, A. Camargo, L. Ayala, M. Zimic, and C. del Carpio, "An algorithm for the estimation of hemoglobin level from digital images of palpebral conjunctiva based in digital image processing and artificial intelligence," *International Journal of Online and Biomedical Engineering,* vol. 20, no. 10, pp. 33–46, 2024. https://doi.org/10.3991/ijoe.v20i10.48331

[10] O. M. Al-Hazaimeh, A. Abu-Ein, N. Tahat, M. Al-Smadi, and M. Al-Nawashi, "Combining artificial intelligence and image processing for diagnosing diabetic retinopathy in retinal fundus images," *International Journal of Online & Biomedical Engineering (iJOE)*, vol. 18, no. 13, pp. 131–151, 2022. https://doi.org/10.3991/ijoe.v18i13.33985

[11] T. Wu, W. Wu, Y. Yang, F. L. Fan, and T. Zeng, "Retinex image enhancement based on sequential decomposition with a plug-and-play framework," *IEEE Trans. Neural Netw. Learn. Syst.,* 2023. https://doi.org/10.48550/arXiv.2210.05436

[12] G. Dimauro, R. Maglietta, T. Bai, and S. Kasiviswanathan, "Eyes-defy-anemia," *IEEE Dataport,* 2022. https://doi.org/10.21227/t5s2-4j73

[13] G. Dimauro, L. Baldari, D. Caivano, G. Colucci, and F. Girardi, "Automatic segmentation of relevant sections of the conjunctiva for non-invasive anemia detection," in *2018 3rd International Conference on Smart and Sustainable Technologies (SpliTech)*, 2018, pp. 1–5. https://doi.org/10.23919/SpliTech.2018.8439608

[14] R. C. Gonzalez and R. E. Woods, *Digital Image Processing*. London: Pearson, 2018.

[15] S. P. Chatzis, "On the efficacy of fuzzy and neuro-fuzzy techniques in dealing with imprecise image data," *Neurocomputing*, vol. 71, nos. 10–12, pp. 1899–1907, 2008. https://doi.org/10.1016/j.neucom.2007.12.030

[16] A. R. Weeks, *Fundamentals of Electronic Image Processing*. Bellingham, WA: SPIE Optical Engineering Press, 1996. https://doi.org/10.1117/3.227778

[17] K. Zuiderveld, "Contrast limited adaptive histogram equalization," in *Graphics Gems IV*, P. S. Heckbert, Ed., Academic Press, 1994, pp. 474–485. https://doi.org/10.1016/B978-0-12-336156-1.50061-6

[18] J. A. Stark, "Adaptive image contrast enhancement using generalizations of histogram equalization," *IEEE Transactions on Image Processing*, vol. 9, no. 5, pp. 889–896, 2000. https://doi.org/10.1109/83.841534

[19] S. Kasiviswanathan, T. Bai Vijayan, L. Simone, and G. Dimauro, "Semantic segmentation of conjunctiva region for non-invasive anemia detection applications," *Electronics*, vol. 9, no. 8, p. 1309, 2020. https://doi.org/10.3390/electronics9081309

[20] N. N. Gharaibeh, O. M. Al-Hazaimeh, B. Al-Naami, and K. M. O. Nahar, "An effective image processing method for detection of diabetic retinopathy diseases from retinal fundus images," *International Journal of Signal and Imaging Systems Engineering*, vol. 11, no. 4, pp. 206–216, 2018. https://doi.org/10.1504/IJSISE.2018.093825

[21] C. Yu, J. Wang, C. Peng, C. Gao, G. Yu, and N. Sang, "Bisenet: Bilateral segmentation network for real-time semantic segmentation," in *Proceedings of the European Conference on Computer Vision (ECCV),* 2018, pp. 325–341. https://doi.org/10.48550/arXiv.1808.00897

[22] O. Ronneberger, P. Fischer, and T. Brox, "U-Net: Convolutional networks for biomedical image segmentation," in *Medical Image Computing and Computer-Assisted Intervention – MICCAI 2015*, in Lecture Notes in Computer Science, N. Navab, J. Hornegger, W. M. Wells, and A. F. Frangi, Eds., vol. 9351, Springer, Cham, 2015, pp. 234–241. https://doi.org/10.1007/978-3-319-24574-4_28

[23] S. Pahwa, A. Kaur, P. Dhiman, and R. Damaševičius, "ConjunctiveNet: An improved deep learning-based conjunctive-eyes segmentation and severity detection model," *International Journal of Intelligent Computing and Cybernetics*, vol. 17, no. 4, pp. 783–804, 2024. https://doi.org/10.1108/IJICC-04-2024-0189

[24] X. Jiang and C. Xu, "Deep learning and machine learning with grid search to predict later occurrence of breast cancer metastasis using clinical data," *J. Clin. Med.*, vol. 11, no. 19, p. 5772, 2022. https://doi.org/10.3390/jcm11195772

[25] H. Noh, S. Hong, and B. Han, "Learning deconvolution network for semantic segmentation," in *2015 IEEE International Conference on Computer Vision (ICCV)*, 2015, pp. 1520–1528. https://doi.org/10.1109/ICCV.2015.178

[26] E. Purwanti, H. Amelia, W. Winarno, M. A. Bustomi, M. A. Yatijan, and R. N. Putri, "Anemia detection using convolutional neural network based on palpebral conjunctiva images," in *2023 14th International Conference on Information & Communication Technology and System (ICTS), Surabaya, Indonesia,* 2023. https://doi.org/10.1109/ICTS58770.2023.10330869

[27] P. Branco, L. Torgo, and R. Ribeiro, "A survey of predictive modelling under imbalanced distributions," *arXiv preprint arXiv:1505.01658*, 2015. https://doi.org/10.48550/arXiv.1505.01658

[28] A. Garcia-Garcia, S. Orts-Escolano, S. Oprea, V. Villena-Martinez, and J. Garcia-Rodriguez, "A review on deep learning techniques applied to semantic segmentation," *arXiv preprint arXiv:1704.06857*, 2017. https://doi.org/10.48550/arXiv.1704.06857

[29] M. A. Valles-Coral, J. R. Navarro-Cabrera, L. Pinedo, R. Injante, L. K. Quintanilla-Morales, and M. E. Farro-Roque, "Non-invasive detection of iron deficiency anemia in young adults through finger-tip video image analysis," *International Journal of Online and Biomedical Engineering (iJOE)*, vol. 20, no. 14, pp. 53–70, 2024. https://doi.org/10.3991/ijoe.v20i14.50141

[30] S. G. Vázquez, N. Barreira, M. G. Penedo, M. Saez, and A. Pose-Reino, "Using retinex image enhancement to improve the artery/vein classification in retinal images," in *Image Analysis and Recognition (ICIAR 2010)*, in Lecture Notes in Computer Science, A. Campilho and M. Kamel, Eds., vol. 6112, Springer, Berlin, Heidelberg, 2010, pp. 47–56. https://doi.org/10.1007/978-3-642-13775-4_6

7 AUTHORS

Jose Humberto Fuentes-Beingolea obtained his degree in Electronic Engineering from Universidad Nacional de San Antonio Abad del Cusco (UNSAAC), Peru. His research develops technological solutions for social advancement using data analytics, artificial intelligence, and image processing. As an associate researcher at LIECAR-UNSAAC, he integrates advanced computational methods with community-focused projects (E-mail: 131358@unsaac.edu.pe).

Facundo Palomino-Quispe earned his Bachelor's in Electronic Engineering from the Private University of Tacna, Peru, and completed an M.Sc. with a focus on Automation and Instrumentation, followed by a Ph.D. in Mechatronics Engineering from the National University of San Agustín of Arequipa (UNSA). Currently, he is a professor at Universidad Nacional de San Antonio Abad del Cusco (UNSAAC) and

directs the LIECAR Laboratory. His research spans mobile robotics, control systems, automation, artificial intelligence, and embedded systems.

Julio Cesar Herrera-Levano finished his degree in Electronic Engineering from Universidad Nacional del Callao and an M.Sc. in Electronic Engineering with a specialization in Automation and Instrumentation from Universidad Nacional San Agustín de Arequipa. A RENACYT Level VII researcher, he has taught at the National University of San Antonio Abad del Cusco (UNSAAC) since 2014. With 25 years in telecommunications, his work advances high-impact research in mobile spectral analysis and SDR evaluation.

Willy Vargas-Mateos earned his Bachelor's degree in Electronic Engineering from the National University of San Marcos (2006) and an M.Sc. in Telematics from the National University of Engineering (2018). Currently pursuing a Ph.D. in Mechatronics Engineering at the National University of San Agustín of Arequipa, he serves as a full-time assistant professor at Universidad Nacional de San Antonio Abad del Cusco. His research addresses proactive conversational agents, decision-support algorithms, and multi-agent reactive repair systems.

Ruben Florez, graduated as an Electronic Engineer from the Universidad Nacional de San Antonio Abad del Cusco (UNSAAC) in 2024. is an assistant professor in the Department of Electronic Engineering and a RENACYT Level VI researcher at LIECAR, and his expertise spans machine learning, deep learning, computer vision, and digital image processing. His work focuses on robotics, health, and cymatics applications. Recognized nationally and internationally, his research advances innovative solutions for real-world challenges.

Ana Beatriz Alvarez completed her degree in Electronic Engineering from Universidad Nacional del Altiplano, Puno, Peru, in 2000, and completed her M.Sc. and Ph.D. in Electrical Engineering at the University of Campinas (UNICAMP) in 2005 and 2011, respectively. A former postdoctoral researcher at UNICAMP, she has been a research professor at the University of Acre (UFAC) since 2013 and has led the PAVIC-Lab since 2022. Her research focuses on computational intelligence, machine learning, and computer vision, emphasizing image restoration and quality improvement.